ELSEVIER

Earth and Planetary Science Letters 209 (2003) 71–83

EPSL

www.elsevier.com/locate/epsl

Seismic detection of sublithospheric plume head residue beneath the Pitcairn hot-spot chain

Sebastian Rost *, Quentin Williams

Department of Earth Sciences, Center for the Study of Imaging and Dynamics of the Earth, University of California Santa Cruz, 1156 High Street, Santa Cruz, CA 95064, USA

Received 15 September 2002; received in revised form 29 January 2003; accepted 5 February 2003

Abstract

We study array seismograms of French nuclear explosions from two islands in French Polynesia and use these to constrain the structure in the upper mantle beneath the islands. Seismograms of nuclear explosions on the hot-spot-related Fangataufa atoll show discrete, large-amplitude P-coda phases which are not observed in recordings of explosions on Mururoa, an atoll ~40 km to the north. The source for these P-coda phases is located beneath the Fangataufa atoll, indicating that structural heterogeneities are present in the oceanic upper mantle in this region on very small scale lengths. Synthetic seismograms for models of the upper mantle beneath Fangataufa require a layer with P-wave velocity elevated by ~10% between depths of 51 and 85 km with a sharp termination in the north, possibly at the Austral Fracture Zone, to match these P-coda phases. Few mineralogic scenarios exist that can explain this structure, and the properties of this layer imply that extensive enrichment in garnet occurs in this depth range. The garnet-enriched layer is likely of similar origin to the well-known xenolithic 'garnet megacryst' suite found in kimberlitic regions. We propose a model for the formation of the Fangataufa and Mururoa atolls involving garnet-enriched zones being generated at depth through magmatic processes at the Pitcairn plume head. Thus, the initiation of hot-spots could produce complex geochemical and structural heterogeneities at depth in the suboceanic mantle.

Keywords: oceanic lithosphere; hot-spots; mantle plumes; high-velocity zones; seismology

1. Introduction

From 1966 to 1996, France tested nuclear bombs on two islands in French Polynesia. The Mururoa (MUR) and Fangataufa (FAN) atolls are located in the vicinity of the South Pacific superswell [1] and are part of the Pitcairn volcanic chain, a young (~10 Ma) volcanic island chain produced by the Pitcairn hot-spot [2] now located 90–100 km southeast of Pitcairn island [3] and ~1000 km southeast from MUR and FAN (Fig. 1). The ages of MUR and FAN are close to the maximum proposed age of the Pitcairn hot-spot, so they likely were generated at the initiation of this hot-spot chain [2]. MUR formed 10.42 ± 0.1 to 11.06 ± 0.11 Ma ago [2,4,5] and is located on the Austral Fracture zone (AFZ) (Fig. 1), which divides ~41 Ma old oceanic lith-

* Correponding author. Tel.: +1-831-459-1437; Fax: +1-831-459-3074.
E-mail addresses: srost@es.ucsc.edu (S. Rost), qwilliams@earthsci.ucsc.edu (Q. Williams).

0012-821X/03/$ – see front matter
doi:10.1016/S0012-821X(03)00075-X

osphere to the north from ~34 Ma old lithosphere to the south [6]. Unlike most other oceanic islands MUR is elongated along a N80° azimuth, probably due to channeling of volcanism along the AFZ [7,8]. FAN was formed 10.12 ± 0.10 to 12.44 ± 0.24 Ma ago [2,9] and is located ~40 km south of MUR and AFZ on ~34 Ma old lithosphere, and shows a roughly hexagonal form approximately half the size of MUR. Both atolls are located on a small oceanic swell ~200 km by 150 km striking S80°W that is approximately 1000 m shallower than the surrounding ocean floor [10]. French nuclear devices were detonated on both islands in 0.5–1.1 km deep bore-holes in the basaltic bodies of the volcanos beneath the coral rim and lagoon of both islands, with MUR as the main test site [11]. The exact locations of the tests were not published by the French Commissariat à l'Energie Atomique, but the atolls are quite small, so that an assignment of the explosions to the islands can be uniquely made (Table 1). Therefore, these explosions provide an unusual opportunity to interrogate the deep structure of oceanic atolls.

Although both islands appear to lie on the same hot-spot track, their lavas and associated xenoliths are geochemically and petrologically distinct [12]. Both islands have been sampled extensively in bore-holes up to 1100 m deep [9,12–14]. MUR's basalts are highly alkaline, and hydrous phases, such as micas and amphiboles, are present in xenoliths [7,13]. In contrast, FAN's basalts are quite conventional for oceanic hot-spot magmatism: initially tholeiitic basalts, followed by a veneer of alkali basalts. The anomalous petrology of MUR rocks has led the association of this island with the Pitcairn hot-spot to be questioned, and a genetic connection with the AFZ has instead been proposed [13,14].

The first tens of seconds of the seismograms of explosions from the two islands are very different, with FAN events showing two dominant P-coda phases. We can model the P-coda phases by introducing a layer with a high ($\Delta v_p \sim +10\%$) P-velocity beneath FAN that is absent beneath MUR. Other sources for the coda phases from FAN, such as the impact of the overburden after its ballistic flight or a reverberation in the water column, can be ruled out due to both travel time and amplitude discrepancies.

Our mineralogic modeling shows that a high percentage of garnet is the only possible means of generating such a large velocity jump in the oceanic upper mantle. We develop a model of

Table 1
French nuclear explosions at MUR and FAN

Event #	Origin		Lat.	Lon.	m_b
			[°]	[°]	
1[a]	1996 January 27	21:29:57.8	−22.240	−138.820	5.3
2	1995 December 27	21:29:58.0	−21.880	−138.970	5.1
3	1995 November 21	21:29:58.1	−21.990	−139.030	4.8
4	1995 October 27	21:59:58.2	−21.890	−138.980	5.4
5[a]	1995 October 01	23:29:58.0	−22.250	−138.740	5.4
6	1995 September 05	21:29:58.4	−21.850	−138.840	4.8
7[a]	1988 November 30	17:55:00.0	−22.233	−138.740	5.5
8	1987 November 19	16:31:00.2	−21.845	−138.941	5.7
9	1986 May 30	17:25:00.1	−21.862	−138.948	5.5
10	1980 July 19	23:47:00.0	−21.861	−138.934	5.7
11[a]	1990 November 14	18:11:58.0	−22.258	−138.805	5.5
12[a]	1990 June 26	17:59:58.2	−22.215	−138.841	5.5
13[a]	1989 November 27	17:00:00.0	−22.250	−138.722	5.5
14[a]	1991 May 29	18:59:58.2	−22.256	−138.794	5.5

Origin time and location of explosions are taken from the Preliminary International Data Center (PIDC) Database of the Comprehensive Nuclear Test-Ban Treaty. m_b, body wave magnitude.
[a] Fangataufa events.

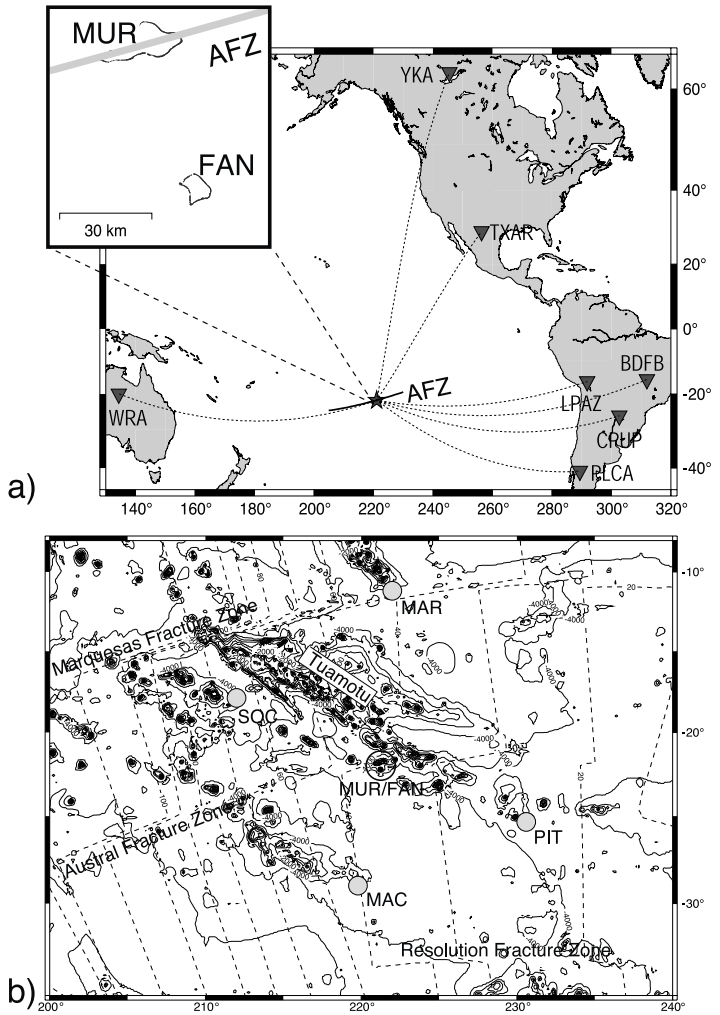

Fig. 1. (a) Source–receiver combinations. The stations used are marked by triangles (BDFB: Brasilia, Brasil; LPAZ: La Paz, Bolivia; CPUP: Villa Florida, Paraguay; PLCA: Paso Flores, Argentina; TXAR: Texas Array, USA). Mainly data of the small-aperture, short-period, vertical arrays of Yellowknife (YKA, Canada) and Warramunga (WRA, Australia) are used. The insert shows the form and location of MUR and FAN. Both islands are atolls with a coral rim and lagoon. The Austral Fracture zone (AFZ) strikes N80°E. MUR and FAN are ~40 km apart. (b) Bathymetric map of the surroundings of MUR/FAN in French Polynesia. The 500 m isolines are given as solid lines. The dashed lines give lithospheric ages [6]. The Austral and Marquesas Fracture zones are clearly visible in lithospheric age. Presumed hot-spots of the region are marked by gray circles (SOC: Society; MAC: MacDonald; MAR: Marquesas; PIT: Pitcairn). MUR and FAN are located in the center of the figure.

the hot-spot-related volcanism at these two islands that explains the geochemical, mineral-physical and seismological data.

These observations demonstrate that the oceanic upper mantle can be heterogeneous on relatively small scale lengths, and that hot-spots are able to produce geochemical heterogeneities that, when entrained into Earth's convective mantle, could produce geochemical signatures that resemble subduction-generated heterogeneities.

2. Seismological data

We study recordings of the small-aperture, short-period seismological arrays in Yellowknife

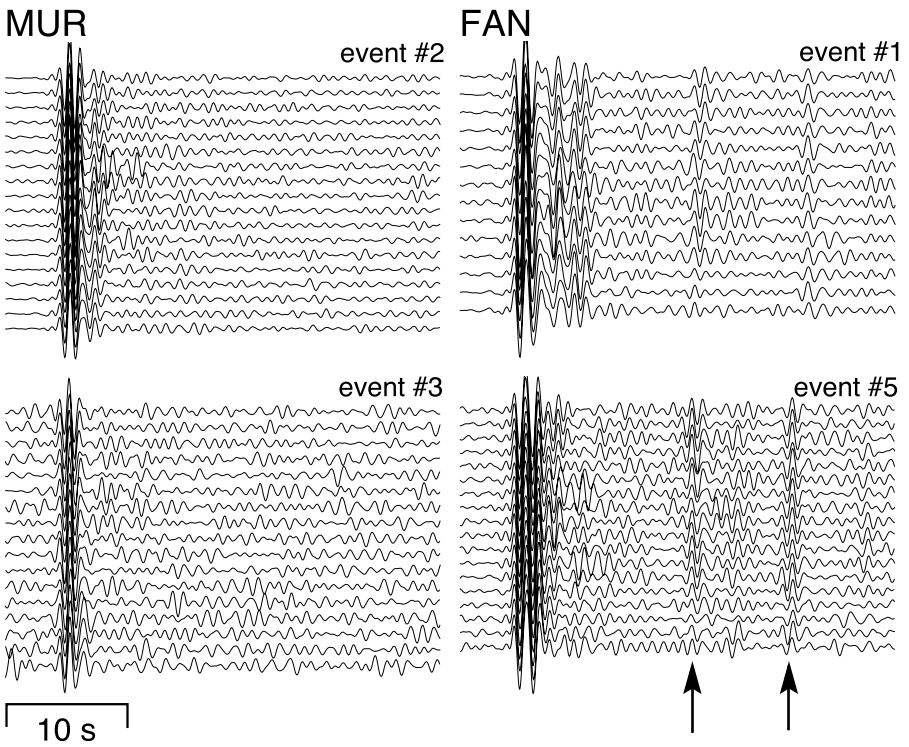

Fig. 2. YKA recordings of explosions in MUR and FAN (events 2, 3, 1, 5) of the 1995/1996 explosion series. Shown are band-pass-filtered seismograms (fourth-order bandpass with cut-off frequencies of 0.5 and 1.4 Hz). All seismograms are normalized to the first arrival. The two large onsets (marked by arrows) in the P-coda at ~16 and ~24 s are clearly visible for the FAN explosions. In contrast, the coda of MUR events is very simple. The polarity of the 16 s phase is opposite to the P-onset, whereas the 24 s phase has the same polarity.

and Warramunga (YKA and WRA, respectively), located in northern Canada and Australia (Fig. 1). Epicentral distances from MUR and FAN to the two arrays are similar with $\Delta_{YKA} = 86.4°$ and $\Delta_{WRA} = 79.8°$. Both arrays have apertures of ~20 km and 18 and 20 vertical, short-period stations, respectively. WRA is built in an L-shaped configuration, whereas YKA is cross-shaped. Both arrays were built to monitor nuclear explosions globally and have operated since the early 1960s. They are especially sensitive to high-frequency P-waves from teleseismic distances and are part of the International Monitoring System to determine compliance with the Comprehensive Nuclear Test Ban Treaty.

Fig. 2 shows recordings from YKA for explosions at MUR and FAN. For event location we use the database of the Prototype International Data Center (PIDC). The differences of the seismograms recorded at the same stations from the two closely spaced atolls are striking. The YKA recordings from explosions on MUR show a very simple P-coda, whereas two large-amplitude P-coda phases at ~16 and ~24 s are visible for FAN explosions. The events are recorded at the same stations and the difference in arrival angle is negligible. Therefore, a receiver side structure as the source for these phases can be completely ruled out. The paths of P from MUR→YKA and FAN→YKA are very similar. The P-wave turns ~300 km above the CMB, so that any structural difference along the path in the deep mantle is very unlikely and highly heterogeneous regions of the mantle like D″ are not sampled by the P-waves. The source for the large coda phases is thus most likely located in the direct vicinity of the atolls. Due to the explosive origin of the seismic energy, the source mechanism is simple and

any systematic difference of source mechanism can be ruled out. The almost circular form and small size of FAN rules out the possibility of an energetic reverberation within the volcanic edifice. Moreover, surface-wave to P-wave conversions in the atoll would arrive earlier in the seismogram [8], as would the impact of the overburden above the shot-point after its ballistic flight. Synthetic seismograms show that phases like PmP (Moho reflection) and Pm_wP (Moho reflection and an additional leg in the water column) would arrive earlier in the coda. Pm_wP arrives ~11.3 s after P for a 15 km deep Moho and a water depth of 4 km and with much smaller amplitude than observed in the data. Shallower Moho depths would increase the time discrepancy. We also expect that the ballistic flight time would be the same for explosions on both islands, since no difference in hypocentral depth is observed. Reverberations in the water column should also be identical between the two islands, since water depth around both atolls is very similar. We constrained the origin of the additional phases using frequency–wavenumber analysis [15], and no azimuthal deviation from the great-circle path was resolvable. Both phases show P-wave slownesses, indicating that the coda phases originate close to the atolls.

We calculated synthetic seismograms using the reflectivity method [16] for a source–receiver combination analogous to FAN→YKA and an array in YKA configuration. Fig. 3 shows a comparison between data (traces 1–6) and some synthetic seismograms (traces 7–15). The synthetic seismograms show that the FAN explosions are best modeled by models including a high-velocity

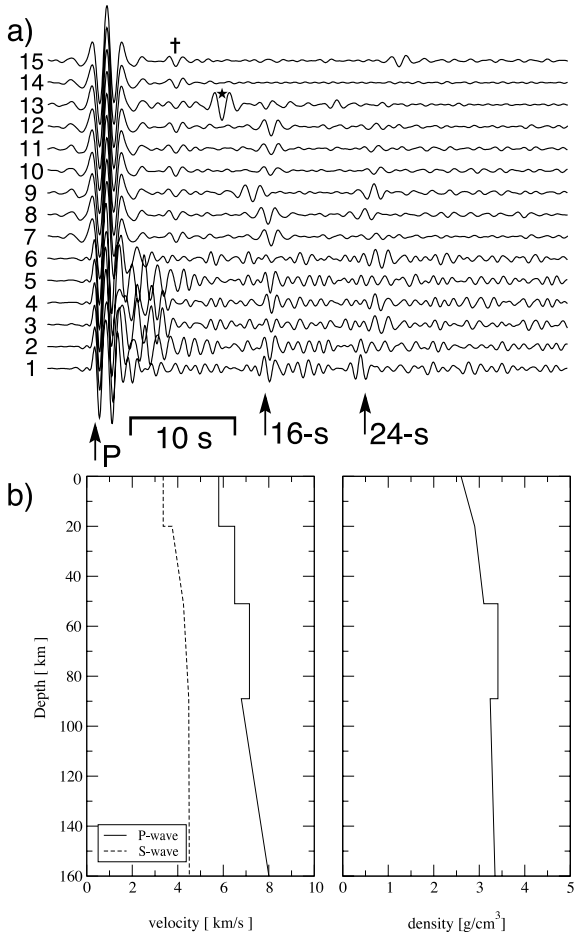

Fig. 3. (a) Data and synthetics beam traces for Fangataufa events recorded at YKA. Traces 1–6 are array beam traces for events 5, 11, 12, 1, 13, 14, respectively. All these events are FAN explosions. Traces 7–15 are synthetic beam traces calculated using the reflectivity method [16] for the YKA→FAN source–receiver combination. The array used in the calculation of the synthetic seismograms has the same configuration as YKA. We use an altered IASP91 model that lacks the strong Moho discontinuity, and therefore lacks the strong arrival from this discontinuity. The synthetic seismograms calculated using the original IASP91 and the modified IAPS91 models are shown as traces 13 and 14, respectively. The asterisk in trace 13 marks the strong arrival from the IASP91 Moho, an arrival we do not observe in the data and which is lacking in the modified model. The cross marks the arrival of the modeled Moho phase in our modified model. The data are best modeled by models containing a high-velocity layer (HVZ) at depth. Trace 7 shows the resulting seismogram for a HVZ between 51 and 89 km with a +20% and −10% impedance contrast, respectively. The model for trace 8 shows a +20% impedance change at 50 km and a −15% change at 85 km and the model for trace 9, ±20% changes at 45 and 89 km. Traces 9–12 show seismograms for HVZ between 51 and 89 km with +10% and −10% impedance changes (trace 10); +15% and −10% (trace 11) and +20% and −10%. We do not have control on the velocity structure in the HVZ, since the internal velocity structure has a minor effect on waveforms and travel times. Trace 15 shows a calculation for a 10% low-velocity layer between 50 and 88 km. This seismogram lacks the prominent onset at 16 s. (b) Best fitting S- and P-wave velocities and density model for HVZ.

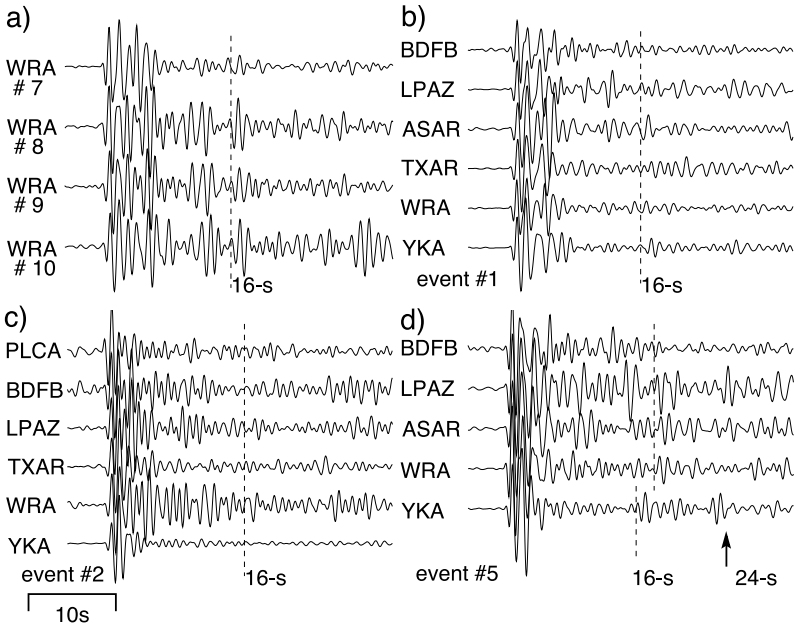

Fig. 4. (a) WRA beam traces of events at FAN (event 7) and MUR (events 8–10). All events show the 16 s phase (dashed line) and some evidence for a 24 s phase. All events are normalized to the P amplitude. The FAN event shows only very small P-coda amplitudes, which might be related to the small P amplitudes for MUR events recorded at WRA [19]. (b–d) Recordings for three different events at FAN (b,d) and MUR (c). The 16 s phase is marked by the dashed lines. Some recordings show a phase with the correct travel time and amplitude, but the single-station data quality is in general worse than for the array. For arrays (WRA, ASAR, TXAR) array beam traces are shown. ASAR is the Alice Springs array in central Australia.

zone (HVZ) beneath the atoll. The observed coda arrivals at 16 and 24 s are identified as reverberations between the upper boundary or lower boundary of the HVZ and the surface (Fig. 5), i.e. $P_{51}pP$ and $P_{85}pP$, for the best-fitting model. The one-dimensional reference Earth model IASP91 [17] (trace 13 in Fig. 3) is not able to produce the large coda phases, but predicts a large arrival ~10 s after P, which is not observed in the data. This predicted phase is due to the strong P-wave discontinuity at 35 km depth in IASP91. For the modeling, we use a modified IASP91 model, which lacks this boundary but has a 12% velocity jump at 20 km and the HVZ at greater depths. The precise depth of this simulated Moho only affects the calculated waveforms near the direct P arrivals and has no resolvable effect at time greater than ~8 s. The synthetic waveforms of the altered velocity model are very similar to the data, although IASP91 is a mainly continental model. If additional phases observable in the FAN explosions are due to the standard discontinuities present in oceanic lithosphere, we would expect similar phases with larger differential time to P also in the MUR explosions, which are not observed. The larger differential travel time would come from a thickening of the lithosphere due to the advanced cooling of the older oceanic lithosphere sampled by the MUR explosions. The model without a HVZ is unable to produce the prominent coda arrivals at 16 and 24 s (trace 14). Traces 7 and 8 extremely accurately reproduce the observed 16 and 24 s arrivals. These models incorporate a layer with an approximately 10% elevation in P-wave velocity and density initiating around 50 km depth, and tapering to a 10–15% impedance contrast between 85 and 90 km depth. The depth of the lower discontinuity is less well-determined than that of the upper discontinuity, because the travel times of the 24 s phase vary by ~2 s between different explosions. Additionally, the amplitudes of the 24 s phase vary between the different explosions. This could be the result of either a fuzzy lower boundary of

the HVZ, or small-scale topography on the lower boundary.

Synthetic tests show that the upper boundary of the HVZ must be very sharp, with the velocity change occurring over less than 2 km, and the upper boundary seems to be locally flat, as indicated by the consistent travel times and amplitudes of the 16 s phase. The 24 s phase ($P_{85}pP$) shows more time variation and lower amplitudes, making both the depth and amplitude of the impedance jump at the lower boundary less precisely determined.

The uppermost trace of Fig. 3 shows the result for a low-velocity zone between 50 and 88 km. Such reduced velocity models are clearly not able to produce the large 16 s phase. Low-velocity zones are common features in the uppermost mantle [18] at depths of 60–200 km and are thought to be produced by the transition from the rheologically defined lithosphere to the asthenosphere. The feature observed beneath FAN is clearly not in agreement with a low-velocity zone. Our models are only slightly sensitive to the velocity gradient within the HVZ and all models shown here have no velocity and density increase or decrease in the HVZ. A normal velocity gradient within the HVZ would alter the inferred depth of the lower boundary slightly. Fig. 4 shows additional data from stations in Australia, South and North America that are used to determine the lateral extent of the high-velocity body that generates the additional P-coda phases. Fig. 4a shows WRA beam traces of explosions on FAN (top trace, event #7) and MUR (events #8 to #10). These recordings show evidence for the 16 and 24 s phase both in MUR and FAN explosions. The identification of the coda phases in WRA data is difficult, because the incoherent coda amplitude for WRA recordings from explosions at MUR and FAN relative to the coherent P-arrivals is about four times higher than in YKA recordings [19,20]. The high relative coda amplitudes are due to an amplitude reduction of the first arrival at WRA rather than an increase in the coda amplitude [19]. Therefore, the WRA amplitude pattern produces more complex seismograms. Nonetheless, since Fig. 4a shows array beam traces, the coda phases stack coherently across the array and

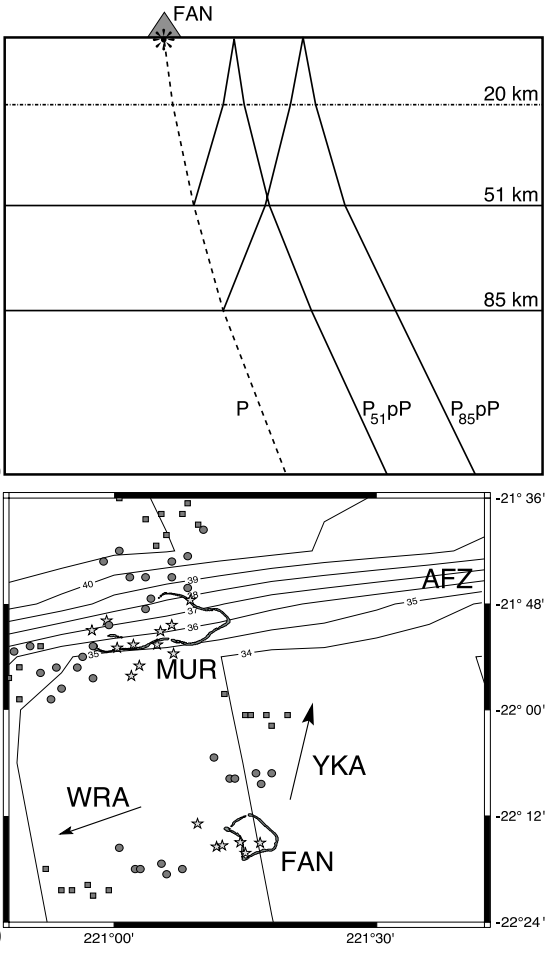

Fig. 5. (a) Sketch of ray paths for phases P, $P_{51}pP$ and $P_{85}pP$. The phases $P_{51}pP$ and $P_{85}pP$ are reflections from the upper and lower boundary of the high-velocity body detected beneath FAN. They arrive 16 and 24 s after the main P arrival at YKA. (b) Location of the reflection points of $P_{51}pP$ (circles) and $P_{85}pP$ (squares) towards YKA and WRA for the nuclear explosions (stars). The solid lines give the lithospheric age in Myr [6]. The path from MUR to YKA samples older lithosphere north of AFZ, whereas MUR→WRA, FAN→WRA and FAN→YKA sample young lithosphere or the fracture zone.

the 16 s phase can be easily identified, proving that the high-velocity body extends to the west of FAN and MUR, making a termination of the layer at the AFZ likely. Fig. 4b,d shows recordings from stations in North and South America and Australia of explosions on FAN, while Fig. 4c shows recordings of an explosion on MUR.

The South American stations (BDFB, LPAZ, PLCA) are single stations, which prevents array processing for these stations. Therefore, the identification of the 16 and 24 s phases is more difficult. Phases arriving in this time window might be reverberations or conversions from discontinuities beneath the stations. The stations ASAR (Australia) and TXAR (USA) are mini-arrays that enable array processing, but have very similar azimuths as the paths from MUR/FAN to WRA and YKA, and therefore do not yield much additional information. In spite of the low quality of the data from the South American stations we find evidence for the 16 s phase in these recordings. Many of these stations seem to have a coherent onset with the appropriate travel time. Therefore, we speculate that the high-velocity body also extends to the east of the two atolls, and thus a lateral extent of $\sim$50 by $\sim$50 km is likely.

The HVZ detected below FAN disappears to the north on a scale length of $\leq$30 km, since the P-coda phases $P_{51}pP$ and $P_{85}pP$ cannot be detected beneath MUR on paths to YKA. It is likely that the northern boundary of the HVZ is the AFZ: The detection of the coda phases from MUR and FAN to WRA and to some of the South American stations indicates an extension of the HVZ to the east and the west, approximately paralleling the fracture zone, while the path from MUR to YKA definitely samples normal oceanic mantle. Any extension of the HVZ to the south cannot be determined since no recordings from Antarctica of the explosions exist. We searched the ISC catalog for identifications of additional phases in the P-coda for these explosions, with no results in the relevant P-wave distance necessary to determine the extent of this velocity anomaly.

Regional and global gravity data [21,22] and geoid [22] for the MUR–FAN region data were examined for any anomaly in the region, without success. The high-velocity body might be isostatically compensated, or small enough relative to its depth extent that it shows no resolvable signal in the gravity and geoid field. The presence of a heat-flow anomaly could also be indicative of a volcanism-related source of the HVZ. Unfortunately, no heat-flow measurements in close proximity to MUR and FAN exist that might indicate the presence or absence of a heat-flow anomaly [23,24]. Indeed, the young age of the lithosphere and low sediment load render such measurements difficult in this region.

3. Mineralogic modeling

The mineralogic options for generating the high-velocity layer required by the seismic data are restrictive, and thus provide key constraints on the make-up and genesis of this layer. Among plausible rock assemblages, eclogites with mid-ocean ridge basalt chemistry have been calculated to have P-wave velocities elevated by only $\sim$2% (with no change in shear velocity) relative to both pyrolite and harzburgite in the 90 km depth range [25]. Eclogites with chemistries that generate higher garnet contents and corresponding lower amounts of pyroxene have progressively larger P-wave velocity elevations [26]. Yet, even comparatively garnet-rich eclogite compositions do not approach the $\sim$10% P-velocity contrast required to produce the observed postcursors. Indeed, among the major upper mantle minerals, olivine, ortho- and clinopyroxene and garnet, only a dramatic increase in the modal concentration of garnet, significantly in excess of that present within eclogites, can generate changes in P-wave velocity of near 10%. This is a simple consequence of the relative incompressibility of garnets relative to other upper mantle phases. For mantle garnets, typical values of the ambient temperature bulk modulus are 170 ($\pm$3) GPa, while those of olivines are $\sim$130 GPa and pyroxenes lie in the 104–116 GPa range [27]. For comparison, the respective shear moduli of the three phases are 92 ($\pm$3), 82 and 74–78 GPa, with pyropic garnet being about 10% denser than olivine and pyroxene. Accordingly, a 10% increase in P-wave velocity implies a dramatic increase in the garnet concentration (and, relative to eclogites, virtual elimination of the lower-velocity pyroxene concentration).

We model the 10% compressional velocity contrast that we observe at the top of this layer using elastic parameters from Duffy and Anderson [27], evaluated at a depth of 50 km and for an adiabat

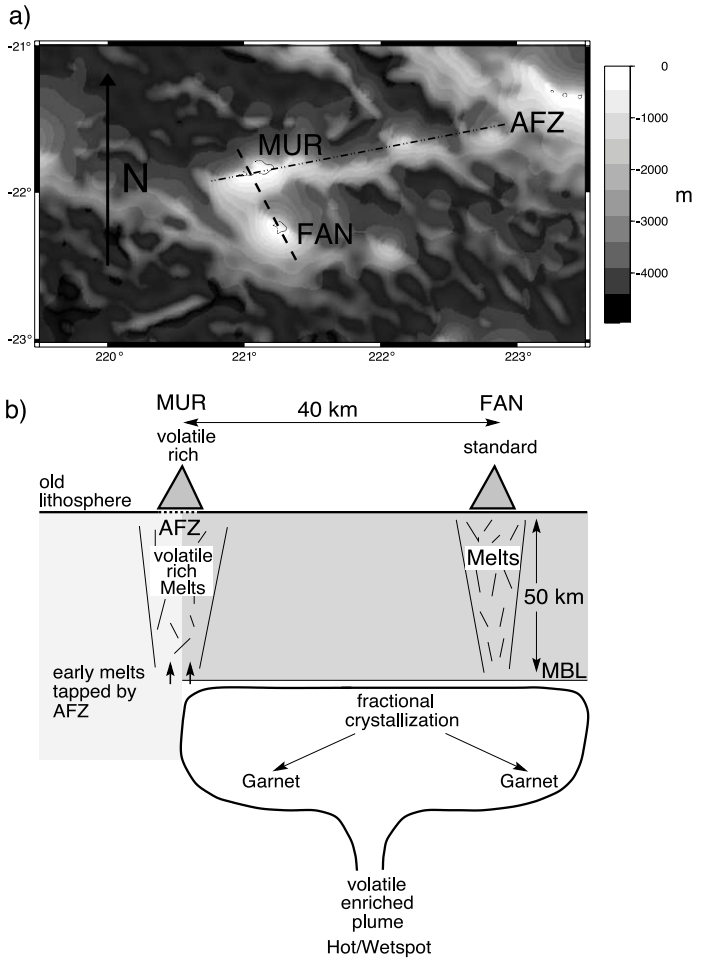

Fig. 6. (a) Topographical map [22] of the MUR/FAN region. The dashed line shows the vertical profile sketched in panel b. The channeling of material along AFZ (dot-dashed line) is clearly visible. (b) Sketch of formation of megacryst suite beneath FAN. Plume material is deposited at ~50 km depth at a mechanical boundary (MBL). The material is either a pulse of material rising along the plume conduit or, more likely, the plume head connected with the start of the Pitcairn volcanic chain. The hot, likely volatile-rich material is trapped at this mechanical boundary. The boundary could be associated with the spinel-to-garnet transition [45], the lower boundary of the lithosphere or a change in viscosity and water content of the mantle material [46]. The initial pulse of plume material is tapped along the weak zone of the AFZ, and generates the volatile-rich minerals and the topography along AFZ associated with MUR (panel a). The trapped, partially molten material undergoes in situ fractional crystallization, building a garnet-rich megacryst layer at depth, while FAN is built up from less volatile-rich melts originating from nearer the center of the plume head.

initiating at 1400°C. We assume that the garnet has an Mg/Mg+Fe number of 0.8, with a grossular component of 10 mol% (our results are only slightly affected by the Ca content of the garnet), and that olivine and pyroxene each have Mg/Mg+Fe numbers of 0.9. A transition between material of approximately harzburgitic chemistry (90% olivine and 10% orthopyroxene) and a layer of between 96 and 100% garnet (with the balance being either olivine or pyroxene) generates a 10% compressional velocity contrast. We model only the velocity contrast at the top of the garnet-rich body, since the reflections from the top are not sensitive to the absolute value of the seismic

velocity but rather provide a robust constraint on the velocity contrast. The amount of garnet can be mildly reduced if the amount of pyroxene in the overlying material is increased: nevertheless, our results indicate that the transition we observe is entirely compatible with a transition from depleted mantle to a lens of nearly pure garnet. Such a pure garnet layer could likely only be generated through fractional crystallization in a magmatic system. In this context, it is notable that slowly ascending picritic magmas, or those arrested at depth, will produce garnet as a major phase during fractional crystallization [28]. This observation led to the proposal that many 'blind conduits may exist at great depths that are filled with alkalic picrites or their fractionation products' [28]. The feature that we document to exist beneath FAN can be explained as a large sill of garnet, generated by fractional crystallization of large quantities of (likely ponded) silicate magma that were present during the genesis of the Pitcairn hot-spot. Additionally, the inferred mineralogy of this layer is fully consistent with the mineralogy of the 'garnet megacryst' suite [29–31]. The garnet megacryst suite is a set of xenoliths composed predominantly of monomineralic garnet, with crystal sizes varying from the cm to m length scale. This suite has been interpreted as the fractional crystallization product of volatile-rich mantle melts, possibly including kimberlites and alnöites [32], an explanation compatible with the observation of hydrous xenoliths on MUR.

4. Discussion

We have presented seismic evidence for a high-velocity body beneath the Fangataufa atoll. Explosions from the Mururoa atoll ~40 km further north prove that the anomaly likely ends at the Austral Fracture zone. Synthetic seismograms show that the velocity in the body is ~10% higher than its overlying layer. Such a velocity increase can only be obtained by a dramatic increase of garnet content within the layer.

In the 1970s and early 1980s, several long-range seismic refraction studies focused on the structure of oceanic lithosphere using ocean-bottom seismometers (OBSs) [33–36] with line lengths of 800–1500 km. Some of these studies found sporadic evidence for a high-velocity layer at depths of 45–75 km [33–36], probably with velocity increases of up to 10%. The study areas were oceanic basins (Lesser Antilles, east Mariana basin and west Philippine Sea) containing old oceanic lithosphere and it has been speculated that this high-velocity layer might be an inherent feature of old oceanic lithosphere [34]. The high-velocity layer was interpreted as being either a layer of anisotropic olivine or a layer with substantial enrichment in garnet [34,37] similar to our modeling, although no source for the garnet increase was previously proposed. It is difficult to obtain a localized 10% P-velocity jump by means of anisotropy alone. Nonetheless, anisotropy might contribute to the observed velocity jump. However, the contribution would be small due to the small inherent anisotropy of garnet.

The early OBS studies have poor signal-to-noise ratio and the data are difficult to interpret. Since the tectonic setting of these studies is different from the one in our study area, we do not necessarily think that the former studies and ours sample the same feature. Nevertheless, the western Pacific and Caribbean regions sampled by the OBS studies are zones that have experienced extensive non-ridge-associated volcanic activity. For comparison, we develop a model of the generation of the HVZ beneath FAN based on the likely origin of MUR/FAN from hot-spot volcanism and the hypothesis that the HVZ is due to a massive enrichment of garnet formed via fractional crystallization.

Based on its geographic position at the start of the Pitcairn chain, the structural heterogeneity beneath FAN is likely a residual feature associated with the genesis of the Pitcairn hot-spot. We propose the following sequential model for the formation of MUR, FAN and the HVZ beneath FAN. The plume head associated with the initiation of the Pitcairn chain (possibly associated with a 'mantle wet-spot' [38]) may have been largely trapped beneath the young lithosphere. Such trapping is in accordance with recent geodynamic modeling of the interaction between ascending plumes and the overlying lithosphere [39,40]. We

assume that the Pitcairn chain arose from the ascent of a relatively small plume, and we do not draw conclusions on the depth of origin of the plume. Nevertheless, the plume ascended into reasonably young lithosphere. Therefore, its thermal buoyancy may have been small relative to the overlying plate. The ascending plume head was likely trapped. Thus, extensive melting and associated fractional crystallization was generated at sub-lithospheric depth. Extensive sub-lithospheric lateral transport of melt (perhaps for many hundreds of km) may have occurred, as has been proposed in other locales [41,42], with early tapping of volatile-rich material at MUR along the AFZ, and movement of large quantities of melt away from the zone of extensive melting near the center of the plume head. Thus, the amount of melt produced at the plume head could have been far greater than that represented by the presently observed volcanic edifices. The seismological data indicate that the HVZ has a sharp lateral termination to the north. This might be due to the thicker (older) lithosphere north of MUR hindering melt transport in this direction. Fractional crystallization of the plume head beneath MUR was likely minimal, since the magma could be tapped through the AFZ and thus transported easily to the surface. Therefore, large quantities of residual fractional crystallization products could progressively accumulate within the trapped head beneath FAN: the estimated volume of the garnet-rich layer that we observe is $40\times50\times50$ $km^3 \approx 10^5$ km^3, likely implying that three to ten times this volume [29] of magma was processed at depth through this region. Indeed, the amount of apparent magmatism in this region is far greater than that represented solely by MUR and FAN. MUR is part of a submarine volcanic range following a N80° trend [7] and a topographic high stretches along the AFZ for nearly 200 km (Fig. 6a), so that the AFZ might have served as a 'leaky fracture zone' for the plume head. The Pitcairn plume head thus appears to have produced distributed regional volcanism, with the primary present-day record of the head being the large magmatically generated feature documented at depth. This sub-surface trapping of liquid and large-scale lateral transport provides a notable contrast with the canonical association of plume heads with flood basalts. In this instance, melt appears to have been emplaced at depth and escaped primarily along zones of weakness. Indeed, if hemorrhaging (as opposed to flooding) of large amounts of magma occurs in other plume heads, then the total mass and heat flux from hot-spots would be underestimated: large-scale sub-lithospheric deposition of hot-spot-related material has not been taken into account in such flux estimations. Therefore, the processes that have occurred beneath Pitcairn may be more representative of those that occur when small plumes impinge on young lithosphere, in which the primary long-term manifestation of the plume head is confined to comparatively small regions of the sub-surface.

Finally, geochemical constraints have indicated that plume-head material may contaminate the source regions of the Pitcairn Island basalts themselves [43]. Regardless of whether this plume-derived material is associated with the genesis of the Pitcairn chain or represents residua from older, recycled heads, our results show that plume heads likely produce large-amplitude heterogeneities at depth in the oceanic mantle on the tens of km length scale: a length scale of importance for geochemical studies of the Earth's mantle [44]. Therefore, plumes appear able to generate geochemically anomalous features at depth that, when entrained into Earth's convecting mantle, can produce geochemical signatures that resemble subduction-generated heterogeneities. Finally, we speculate that such garnet-enriched features could be common beneath the start of hot-spot tracks that lack associated flood basalts.

Acknowledgements

We thank Elise Knittle, Justin Revenaugh, Richard Von Herzen and Thorne Lay for helpful comments and discussions. We thank J. Gaherty and N. Sleep for their constructive reviews. Funding for this study was provided by NSFgrant EAR-9905733. This is CSIDE (formerly Institute of Tectonics) contribution number 459.*[SK]*

References

[1] M.K. McNutt, K.M. Fischer, The south Pacific superswell, in: B. Keating, P. Fryer, R. Batiza, G. Boehler (Eds.), Seamounts, Islands and Atolls, Geophys. Monogr. 43, Am. Geophys. Union, Washington, DC, 1987, pp. 25–43.

[2] V. Clouard, A. Bonneville, How many Pacific hotspots are fed by deep-mantle plumes?, Geology 29 (2001) 695–698.

[3] P. Stoffers, R. Hékinian, D. Ackermann, N. Binard, R. Botz, C.W. Devey, D. Hansen, R. Hodkinson, G. Jeschke, J. Lange, E. van de Perre, J. Scholten, M. Schmitt, P. Sedwick, J.D. Woodhead, Active Pitcairn hotspot found, Mar. Geol. 95 (1990) 51–55.

[4] H. Guillou, P.Y. Gillot, G. Guille, Age (K-Ar) et position des iles Gambier dans l'alignement du point chaud de Pitcairn (Pacifique Sud), C. R. Acad. Sci. Paris 318 (1994) 635–641.

[5] P.Y. Gillot, Y. Cornette, G. Guille, Age (K-Ar) et conditions d'edification du soubassement volcanique de l'atoll de Mururoa (Pacifique Sud), C. R. Acad. Sci. Paris 314 (1992) 393–399.

[6] D. Müller, W.R. Roest, J.-Y. Royer, L.M. Gahagan, J.G. Sclater, Digital isochrons of the world's ocean floor, J. Geophys. Res. 103 (1997) 3211–3214.

[7] G. Guille, G. Goutière, J.F. Sornein, Les Atolls de Mururoa et de Fangataufa, 1. Géologie -Pétrologie - Hydrogéologie, Masson, Paris, 1993.

[8] M. Weber, C.W. Wicks, F. Krüger, G. Jahnke, J. Schlittenhardt, Asymmetric radiation of seismic waves from an atoll - Nuclear tests in French Polynesia, Geophys. Res. Lett. 25 (1998) 1967–1970.

[9] H. Guillou, R. Brousse, P.Y. Gillot, G. Guille, Geological reconstruction of Fangataufa Atoll, South Pacific, Mar. Geol. 110 (1993) 377–391.

[10] W.H.F. Smith, D.T. Sandwell, Global sea floor topography from satellite altimetry and ship depth soundings, Science 277 (1997) 1956–1962.

[11] J. Bouchez, R. Lecomte, Les Atolls de Mururoa et de Fangataufa, 2. Les Expérimentations Nucléaires: Effets Mécaniques, Lumino-thermiques, Electromagnétiques, Masson, Paris, 1995.

[12] D.C. Buigues, Geology and Hydrogeology of Carbonate Islands, Developments in Sedimentology, Elsevier Science, 1997, pp. 433–451.

[13] J.-M. Bardintzeff, J. Demange, A. Gachon, Petrology of the volcanic bedrock of Mururoa Atoll (Tuamotu Archipelago, French Polynesia), J. Volcanol. Geotherm. Res. 28 (1986) 55–83.

[14] J.-M. Bardintzeff, H. Leyrit, H. Guillou, G. Guille, B. Bonin, A. Giret, R. Brousse, Transition between tholeiitic and alkali basalts: Petrographical and geochemical evidence from Fangataufa, Pacific Ocean, and Kerguelen, Indian Ocean, Geochem. J. 28 (1994) 489–515.

[15] E.J. Kelly, Response of seismic arrays to wide-band signals, Linc. Lab. Techn. Note 1967-30, Lincoln Laboratories, 1967.

[16] G. Müller, The reflectivity method: A Tutorial, J. Geophys. 58 (1985) 153–174.

[17] B.L.N. Kennett, E.R. Engdahl, Traveltimes for global earthquake location and phase identification, Geophys. J. Int. 105 (1991) 429–465.

[18] B. Gutenberg, Wave velocities below the Mohorovičić discontinuity, Geophys. J. 2 (1959) 348–352.

[19] A. Douglas, P.D. Marshall, J.B. Young, Seismograms from explosions in the S. Pacific recorded at four arrays, AWE Report O 2/95, Atomic Weapons Establishment, HMSO, London, 1996.

[20] A. Douglas, Comment on: Asymetric radiation of seismic waves from an atoll-Nuclear test in French Polynesia, by M. Weber, C.W. Wicks, Jr., F. Krüger, G. Jahnke and J. Schlittenhardt, Geophys. Res. Lett. 27 (2000) 1061–1062.

[21] V. Clouard, A. Bonneville, H.G. Barsczus, Size and depth of ancient magma reservoirs under atolls and islands of French Polynesia using gravity data, J. Geophys. Res. 105 (2000) 8173–8191.

[22] D.T. Sandwell, W.H.F. Smith, Marine gravity anomaly from Geosat and ERS 1 satellite altimetry, J. Geophys. Res. 102 (1997) 10039–10054.

[23] H.N. Pollack, S.J. Hurter, J.R. Johnson, Heat flow from the Earth's interior: Analysis of the global data set, Rev. Geophys. 31 (1993) 267–280.

[24] R. Anderson, M. Hobart, R. Von Herzen, D. Fornari, Geophysical surveys on the East Pacific Rise-Galapagos Rise system, Geophys. J. R. Astron. Soc. 54 (1978) 141–166.

[25] D. Gubbins, A. Barnicoat, J. Cann, Seismological constraints on the gabbro-eclogite transition in subducted oceanic crust, Earth Planet. Sci. Lett. 122 (1994) 89–101.

[26] G.R. Helffrich, S. Stein, B.J. Wood, Subduction zone thermal structure and mineralogy and their relationship to seismic wave reflections and conversions at the slab/mantle interface, J. Geophys. Res. 94 (1989) 753–763.

[27] T.S. Duffy, D.L. Anderson, Seismic velocities in mantle minerals and the mineralogy of the upper mantle, J. Geophys. Res. 94 (1989) 1895–1912.

[28] C.S. Milholland, D.C. Presnall, Liquidus phase relations in the CaO-MgO-Al_2O_3-SiO_2 system at 3.0 GPa; the aluminous pyroxene thermal divide and high-pressure fractionation of picritic and komatiitic magmas, J. Petrol. 39 (1998) 3–27.

[29] C.R. Neal, J.P. Davidson, An unmetasomized source for the Malaitian alnite (Solomon islands): Petrogenesis involving zone refining, megacryst fractionation and assimilation of oceanic lithosphere, Geochim. Cosmochim. Acta 53 (1989) 1975–1990.

[30] J.J. Hops, J.J. Gurney, B. Harte, The Jagersfontein Cr-poor megacryst suite - towards a model for megacryst petrogenesis, J. Volcanol. Geotherm. Res. 50 (1992) 143–160.

[31] G.R. Davies, A.J. Springs, P.H. Nixon, A non-cognate origin for the Gibeon kimberlite megacryst suite, Namibia: Implications for the origin of Namibian Kimberlites, J. Petrol. 41 (2001) 159–172.

[32] D.J. Schulze, J.R. Valley, D.R. Bell, M.J. Spicuzza, Oxygen isotope variations in Cr-poor megacrysts from kimberlite, Geochim. Cosmochim. Acta 65 (2001) 4375–4385.
[33] A. Hales, C. Helsley, J. Nation, P travel times for an oceanic path, J. Geophys. Res. 75 (1970) 7362–7381.
[34] T. Asada, H. Shimamura, Long-range refraction experiments in deep ocean, Tectonophysics 56 (1979) 67–82.
[35] The LADLE Study Group, A lithospheric seismic refraction profile in the western North Atlantic Ocean, Geophys. J. R. Astron. Soc. 75 (1983) 23–69.
[36] D. Goodman, L. Bibee, Measurements and modelling of possible mantle constituents from a long-line seismic refraction experiment in the West Phillipine Basin, Geophys. J. Int. 106 (1991) 667–675.
[37] H. Shimamura, T. Asada, M. Kumazawa, High shear velocity layer in the upper mantle of the western Pacific, Nature 269 (1970) 680–682.
[38] C.J. Ebinger, N.H. Sleep, Cenozoic magmatism throughout East Africa resulting from impact of a single plume, Nature 395 (1998) 788–791.
[39] N.H. Sleep, Lateral flow and ponding of starting plume material, J. Geophys. Res. 102 (1997) 10001–10012.
[40] L.T. Elkins Tanton, B.H. Hager, Melt intrusion as a trigger for lithospheric foundering and the eruption of the Siberian flood basalts, Geophys. Res. Lett. 27 (2000) 3937–3940.
[41] J.G. Schilling, M. Zajac, R. Evans, T. Johnston, W. White, J.D. Devine, R. Kingsley, Petrologic and geochemical variations along the Mid-Atlantic Ridge from 29 degrees N to 73 degrees N, Am. J. Sci. 283 (1983) 510–536.
[42] N.H. Sleep, Hotspots and mantle plumes; some phenomenology, J. Geophys. Res. 95 (1990) 6715–6736.
[43] M.K. McNutt, D.W. Caress, J. Reynolds, K.A. Jordahl, R.A. Duncan, Failure of plume theory to explain midplate volcanism in the southern Austral islands, Nature 389 (1997) 479–482.
[44] J.D. Woodhead, M.T. McCulloch, Ancient seafloor signals in Pitcairn island lavas and evidence for large amplitude, small length-scale mantle heterogeneities, Earth Planet. Sci. Lett. 94 (1989) 257–273.
[45] A.L. Hales, A seismic discontinuity in the lithosphere, Earth Planet. Sci. Lett. 7 (1969) 44–46.
[46] G. Hirth, D.L. Kohlstedt, Water in the oceanic upper mantle: implications for rheology, melt extraction and the evolution of the lithosphere, Earth Planet. Sci. Lett. 144 (1996) 93–108.